Comprehensive Modeling of Precipitation and Fouling in Turbulent Pipe Flow

ARTICLE *in* INDUSTRIAL & ENGINEERING CHEMISTRY RESEARCH · MARCH 1998

Impact Factor: 2.59 · DOI: 10.1021/ie970559g

2 AUTHORS:

Margaritis Kostoglou
Aristotle University of Thessaloniki
165 PUBLICATIONS **2,064** CITATIONS
SEE PROFILE

Anastasios J. Karabelas
The Centre for Research and Technology, Hel…
288 PUBLICATIONS **4,416** CITATIONS
SEE PROFILE

Comprehensive Modeling of Precipitation and Fouling in Turbulent Pipe Flow

M. Kostoglou and A. J. Karabelas*

Chemical Process Engineering Research Institute and Department of Chemical Engineering, University Box 455, Aristotle University of Thessaloniki, GR 54006 Thessaloniki, Greece

Supersaturation with respect to an active compound triggers several precipitation-related processes that may proceed (essentially concurrently) along the flow path. The interaction between fluid dynamics and physicochemical processes (i.e., nucleation, particle growth, and coagulation) leads to an axial variation of bulk properties (species concentration and particle size distribution) and of ionic and particulate deposition rates at the pipe wall. To simulate this complicated system, very simple hydrodynamics (plug flow) is combined with rather comprehensive modeling of physicochemical phenomena. Considerable effort is devoted to the optimization of computational requirements, thus developing a numerical algorithm efficient and flexible enough to cope with even more demanding future tasks such as the inclusion of mixing. The performance of the model is examined using, as a test case, the precipitation of a sparingly soluble salt under conditions typical for geothermal installations. An extensive study of the effects of the initial saturation ratio and of the tendency for particle coagulation on the deposition rate and on the particle size distribution along the pipe is carried out.

1. Introduction

Precipitation of sparingly soluble salts from flowing (mostly aqueous) solutions is commonly encountered in industrial installations and related equipment. Typical cases include plants processing inorganic compounds (e.g., salts of Ca and Mg), hydrometallurgical units, and water management pipeline networks. Thus, one is quite often concerned with precipitation phenomena occurring in transfer pipelines as well as in all kinds of heat exchangers (heaters, condensers, etc.) and other process equipment (separators, mixers, etc.).

In these cases, the change of a liquid property (e.g., pH, temperature, species concentration) can induce supersaturation with respect to one or more compounds, thus promoting several phenomena that may be classified into two main categories, i.e., *ionic* and *particulate* processes. Figure 1 provides an overview of various physical processes that may occur in the typical case of pipe flow of a supersaturated solution. *Ionic processes* (associated with consumption of ionic species) may take place both in the bulk (particle growth) and right at the pipe wall (ionic deposition). Similarly, particle agglomeration and wall deposition are the respective *particulate processes*. In practical cases involving sparingly soluble compounds, the rates in most of these individual processes tend to be of the same order of magnitude. Therefore, the respective processes may occur *concurrently*, creating very serious difficulties in studying separately each one of them as well as in modeling and predicting the outcome of their complicated interaction. It is pointed out that useful comprehensive models should provide reliable estimates of the spatial (axial) variation of key quantities such as the rate of deposit growth, active species concentration, and particle size distribution. Prediction of the latter necessitates the use of a population balance type of problem formulation.

There is considerable work reported in the literature on various aspects of this problem. A few typical examples are outlined here. Den Ouden and Thomson (1991) employed a simplified form of population balance which cannot address several key issues of the full precipitation problem. Studies of aerosol flow in pipes, where population balance type of formulations are used, include those of Nadkarni and Mahalingam (1985) for laminar and turbulent flow and of Xiong and Pratsinis (1991) for plug flow. Okuyama et al. (1991) and Tandon and Rosner (1996) studied the influence of the particle size distribution on deposition rate and on deposit morphology for CVD. Park and Rosner (1989) treated the effect of coagulation on deposition rate in boundary layer flow around bluff bodies. Rosner and Tassopoulos (1989) studied the influence of the particle size distribution on the particulate deposition rate under several deposition mechanisms. Wachi and Jones (1991) studied precipitation effects in gas/liquid mass transfer by means of population balances. Significant reviews on various aspects of crystallization and precipitation are those of Garside (1985) and Dirksen and Ring (1991).

The present study, though quite general, is motivated by the need to predict the variation of fluid, particle, and deposit properties along the flow path in geothermal installations. The geothermal fluids, depending on their enthalpy and geological origin (e.g., Andritsos and Karabelas, 1991a), are usually rich in inorganic compounds and tend to become supersaturated either by a pH increase (e.g., due to CO_2 flashing) or by temperature reduction (e.g., in the case of heavy metal sulfides). Of significant practical interest here is the prediction of scaling rates, of scale properties, and of bulk solids size distribution which tend to vary significantly along the flow path. Considerable work has been carried out in this laboratory to understand the physicochemical factors influencing these processes and in particular fouling

* Author to whom correspondence is addressed. Telephone: 30-31-996201. Fax: 996209. E-mail: Karabaj@alexandros.cperi.forth.gr.

S0888-5885(97)00559-9 CCC: $15.00
Published on Web 03/03/1998

(Andritsos and Karabelas, 1991b,c). A previous effort to simulate related phenomena, using population balances, is reported by Kostoglou et al. (1995). Although quite comprehensive, this model has definite limitations, as it is focused on simulating a specific experimental setup and on interpreting the respective data, thus obtaining an improved physical understanding. Nevertheless, the achieved fairly good agreement between theory and experiment suggests that the modeling approach is the right one and that it should be exploited further. Therefore, in this study a more general model is presented, covering essentially all the major mechanisms of the individual processes. Furthermore, the new model is characterized by improved flexibility, thus allowing its extension to include realistic aspects of the flow (e.g., mixing effects)—an area of prime interest in precipitation research.

This presentation starts with the basic formulation, followed by a brief description of individual mechanisms. Next, the proposed numerical solution techniques are outlined, and the results are presented in a form as general as possible. Lead sulfide is used as the typical active compound in this study, as it is frequently encountered in geothermal fluids.

2. Problem Formulation

2.1. Physicochemical Processes. A solution of salt A_aB_b is considered, dissociating as follows:

$$aA + bB \leftrightarrow A_aB_b \tag{1}$$

The driving force for precipitation in the fluid bulk, as well as crystallization onto the pipe wall, is the change of the Gibbs free energy

$$\Delta G = -RT \ln S \tag{2}$$

where R is the ideal gas constant, T the absolute temperature, and S the saturation ratio defined as

$$S = \left[\frac{(A)^a(B)^b}{K_{sp}}\right]^{1/(a+b)} \tag{3}$$

The quantities in parentheses denote activities of respective species and K_{sp} is the thermodynamic solubility product of the dissociating salt.

Figure 1 is a schematic of the simultaneously occurring processes, which are promoted by the consumption of ionic species A. The light and heavy lines in this figure correspond to ionic and particulate processes, respectively. For small supersaturations, there is no precipitation in the fluid bulk and ionic species seem to be consumed only through a pipe surface reaction in creating a crystalline deposit (scale). For larger supersaturations, nucleation in the fluid bulk takes place and the ensuing processes of particle growth, through ionic addition and agglomeration, result in a *distribution* of particle sizes. Under these conditions, scale formation on the pipe surface proceeds as a combination of ionic and particulate deposition.

The following assumptions are made in order to mathematically simulate the above processes: (i) plug flow in the pipe; (ii) radially uniform concentration distribution of reacting species; and (iii) particles of spherical shape. The first two assumptions are typical of problems of practical interest, as is the case of tubular chemical reactors (Smith, 1981). The third assumption

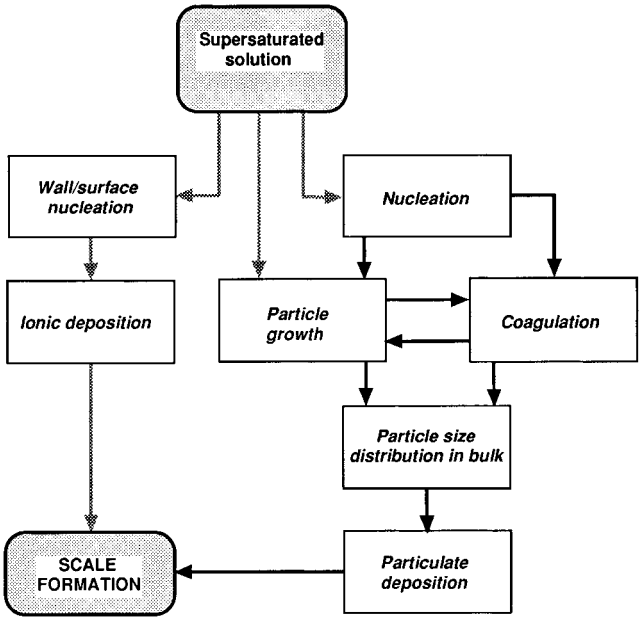

Figure 1. Physical processes occurring in pipe flow of supersaturated solutions.

is valid in the case of fluid particles but is also frequently used for solid particles for convenience. As regards individual particle growth through ionic addition, the nonspherical particle shape (e.g., cubes in the case of PbS) poses no problem and it is usually taken care (quite satisfactorily) with an equivalent diameter. However, the parameters (fractal dimension, radius of gyration, etc.) representing the morphology of aggregates, which are created under the combined action of Brownian motion, fluid shear, and ionic addition, cannot be determined at present. If they become available, they may be incorporated into the population balances in the manner suggested by Koch and Friedlander (1990) or Williams and Loyalka (1991).

A notable feature of the present model is that particle–particle and particle–wall interactions are accounted for, paying particular attention to their influence on quantities of practical interest such as deposition rate. These interactions are introduced into the population balance through the *stability ratio.* In the literature on aerosols (Brock, 1983) and industrial crystallization (Randolph and Larson, 1971), where most of the population balance applications are encountered, either the stability ratio (or collision efficiency) is not taken into account or (if it is) its computation is carried out in such a simple way (Xiong et al., 1992) that it poses no problem. However, in the case of hydrosols, an attempt to accurately calculate the stability ratio W is associated with a considerable increase of computational load. For this reason, until recently, in the relatively few cases where the stability ratio was considered (Reddy et al., 1981) various techniques and/or simplifications were employed. The most common is to compute exactly a reference stability ratio for a specific pair of particles and the ratio for any other pair to be obtained through a simple function of this reference stability ratio (Bogush and Zukoski, 1991; Gianneti, 1993). Hall et al. (1991) have studied the effect of interparticle forces on agglomeration using a Monte Carlo method. Prieve and Lin (1982) have employed a different approach by estimating a mean stability ratio for various particle size distributions. Only in recent studies has a rather accurate computation of W been incorporated into a

population balance in order to predict an evolving particle size distribution due to agglomeration (Tsouris and Scott, 1995; Gardner and Theis, 1996).

Another interesting feature of the present study is the model for computing individual particle growth. This model takes into account surface reaction and the different diffusion rates of various ions. In contrast, such literature models combined with population balances are usually very simple. It is noted that the model employed by Muhr et al. (1995) is an exception, including surface reaction, Ostwald ripening, and effect of chemical complexes; it does not, however, allow for different diffusivities of various ions. On the basis of the present model, it is possible to examine the effect of varying concentration and of ion diffusivities on the rate of individual particle growth.

As pointed out already, the simplest possible fluid mechanical model (of plug flow) is employed here. However, it has been recognized (e.g., Tavare, 1986) that mixing effects (and consequently the flow field) may play a significant role in crystallization and, in particular, in precipitation processes. Typical studies in this field include the influence of limiting phenomenological mixing patterns on the resulting particle size distribution (Garside and Tavare, 1985; Crundwell, 1994). More advanced recent approaches, relating to the flow field, involve the use of time-averaged Navier−Stokes equations in connection with mass conservation and population balances (Seckler et al., 1995), as well as formulations employing relevant probability density functions, as has already been attempted in a similar polymerization problem (Tsai and Fox, 1996). It must be stressed, though, that with these methods the computational load would be extremely heavy; therefore, to make computations tractable, the associated physicochemical model should be as simple as possible. With these considerations in mind, the physicochemical model of the present study covers satisfactorily the physical aspects of the process, being (computationally) sufficiently simple to permit a future extension to more complicated flow models.

2.2. Mathematical Formulation. The system considered can be described by the following equations:

Population balance

$$\frac{\theta f(x,t)}{\theta t} = \frac{1}{2}\int_0^x B(y,x-y)\, f(y,t)\, f(x-y,t)\, \mathrm{d}y - f(x,t)\int_0^\infty B(x,y)\, f(y,t)\, \mathrm{d}y - \frac{\theta G(x,c_A)\, f(x,t)}{\theta x} - D(x)\, f(x,t) + H(c_A)\, \delta(x-\alpha) \quad (4)$$

Mass balance for species (ions) A

$$\frac{\mathrm{d}c_A}{\mathrm{d}t} = -r\rho\int_0^\infty G(x,c_A)\, f(x,t)\, \mathrm{d}x - r\rho\alpha H(c_A) - \frac{4}{d_t}L(c_A) \quad (5)$$

Total mass m of deposit accumulated on the pipe surface over a space time period t

$$\frac{\mathrm{d}m}{\mathrm{d}t} = Q\rho\int_0^\infty xD(x)\, f(x,t)\, \mathrm{d}x + \frac{4Q}{rd_t}L(c_A) \quad (6)$$

where x, y = particle volumes, c_A = concentration of species A, α = nucleus volume, $L(c_A)$ = ionic deposition rate, $D(x)$ = particulate deposition rate, $H(c_A)$ = nucleation rate, $G(x,c_A)$ = volume particle growth rate, $B(x,y)$ = coagulation rate, $f(x,t)$ = particle number concentration density, t = space time along the pipe, ρ = particle density, r = a/(molecular weight of A_aB_b), d_t = pipe diameter, and Q = volumetric flow rate.

Dimensionless quantities are introduced as follows:

$$\bar{x} = \frac{x}{\alpha} \qquad \tau = \frac{t}{t_0} \qquad F(x,t) = \frac{\alpha f(x,t)}{N_0}$$

$$\bar{B}(x,y) = t_0 N_0 B(x,y) \qquad \bar{G}(x,c) = \frac{t_0 G(x,c)}{\alpha}$$

$$\bar{H}(c) = \frac{t_0 H(c)}{N_0} \qquad \bar{D}(x) = t_0 D(x)$$

$$\bar{L}(c) = \frac{4t_0 L(c)}{d_t c_{A0}} \qquad \bar{c}_i = \frac{c_i}{c_{A0}}$$

where the index i designates either A or B, c_{i0} is the inlet concentration of i, t_0 is the total space time of the pipe, and N_0 is a reference total particle number concentration.

The dimensionless form of eqs 4−6 is as follows:

Population balance

$$\frac{\theta F(\bar{x},\tau)}{\theta\tau} = \frac{1}{2}\int_0^{\bar{x}} \bar{B}(\bar{y},\bar{x}-\bar{y})\, F(\bar{y},\tau)\, F(\bar{x}-\bar{y},\tau)\, \mathrm{d}\bar{y} - F(\bar{x},\tau)\int_0^\infty \bar{B}(\bar{x},\bar{y})\, F(\bar{y},\tau)\, \mathrm{d}\bar{y} - \frac{\theta\bar{G}(\bar{x},\bar{c}_A)\, f(\bar{x},\tau)}{\theta\bar{x}} - \bar{D}(\bar{x})\, F(\bar{x},\tau) + \bar{H}(\bar{c}_A)\, \delta(\bar{x}-1) \quad (7)$$

Mass balance

$$\frac{\mathrm{d}\bar{c}_A}{\mathrm{d}\tau} = -A\int_0^\infty \bar{G}(\bar{x},\bar{c}_A)\, F(x,\tau)\, \mathrm{d}\bar{x} - A\bar{H}(\bar{c}_A) - \bar{L}(\bar{c}_A) \quad (8)$$

Deposited mass

$$\frac{\mathrm{d}m}{\mathrm{d}\tau} = AB\int_0^\infty \bar{x}\bar{D}(\bar{x})\, F(\bar{x},\tau)\, \mathrm{d}\bar{x} + B\bar{L}(\bar{c}_A) \quad (9)$$

where

$$A = \frac{N_0\alpha\rho r}{c_{A0}} \qquad B = \frac{Qc_{A0}}{r}$$

The concentration of B can be readily obtained from the local concentration of A through the relation

$$c_B = c_{B0} - \frac{b}{a}(c_{A0} - c_A) \quad (10)$$

The numerical solution of the above system and especially of eq 7 is not an easy task, and there is considerable recent literature on the subject (e.g., Kostoglou and Karabelas, 1994, 1995; Litster et al., 1995). The method of moments (Williams and Loyalka, 1991) can give, under specific conditions, very good results with minimum computational requirements. The general form of the function $F(\bar{x})$ is considered known, and only a few parameters are unknown functions of time. The most usual choice for the form of $F(\bar{x})$ is the logarithmic normal distribution (Cohen and Vaughan, 1971), which may be applicable only if the particle size distribution is unimodal. However, if the active species are produced

by slow chemical reaction, the resulting particle size distribution may be bimodal (e.g., Landgrebe and Pratsinis, 1990). Although this case is typical for aerosols (Megaridis and Dobbins, 1990; Maetzing et al., 1996), it does not appear to be relevant for precipitation processes in liquid media considered here.

The success of the log-normal distribution to simulate Brownian coagulation is well-known (Lee, 1985). For simulating *turbulent* coagulation, there are differing opinions in the literature. Xiong and Pratsinis (1991) studying a realistic problem argue that the log-normal distribution is adequate for simulating turbulent coagulation; on the other hand, Williams (1985) reports that this approach is poor. In the case studied here, the log-normal distribution is considered a good choice because the extent of turbulent coagulation in precipitation processes is usually small in relation to that of Brownian coagulation. For the simulation of particle growth, the log-normal distribution is appropriate except for the case of large dispersivities (Tsang and Rao, 1988) not encountered in precipitation processes.

As regards particle removal, if the rate of removal increases with particle size, the log-normal distribution does not satisfactorily predict the total particle number and mass concentration (see Barret and Jheeta, 1996, for gravitational deposition). For the case of the removal rate decreasing with increasing particle size (e.g., turbulent diffusional deposition, applicable here), comparisons made with exact solutions have shown that the use of log-normal distribution predicts extremely well the total number and mass concentration of the particles. In conclusion, even though there are other more sophisticated approximations such as the bimodal log-normal, the Weibull, and the improved moments method (Barret and Jheeta, 1996), the simple log-normal distribution appears to be overall the best choice for the problem of precipitation, leading to computational stability, simplicity, and efficiency.

The dimensionless moments of the particle size distribution are defined through the relation

$$M_i = \int_0^\infty \bar{x}^i F(\bar{x},\tau)\, \mathrm{d}\bar{x} \tag{11}$$

In particular $N = M_0$ is the total number concentration and $\varphi = M_1$ the total mass concentration of particles. It is considered that the particle size distribution has (at any instance) a log-normal shape

$$F(\bar{x},\tau) = \frac{N}{\sqrt{2\pi\sigma}}\frac{1}{x}\exp\left[-\frac{1}{2\sigma}\ln^2\left(\frac{\bar{x}}{\hat{v}}\right)\right] \tag{12}$$

where $\sigma = \ln(NM_2/\varphi^2)$ is the dispersivity of the distribution and $\hat{v} = (\varphi/N)\mathrm{e}^{-\sigma/2}$ is the median (logarithmic mean) value of the distribution. The following relation is valid for the moments of the log-normal distribution:

$$M_n = N\hat{v}^n \exp\left(\frac{n^2\sigma}{2}\right) \tag{13}$$

To proceed with the method of moments, eq 7 is multiplied by x^i ($i = 0, 1, 2$) and integrated for all values of particle size. Using the relation $\sigma = \ln(NM_2/\varphi^2)$, the following system of differential equations results for the quantities N, φ, σ, c_A, and m:

$$\frac{\mathrm{d}N}{\mathrm{d}\tau} = -R_0 - \frac{1}{2}J_0N^2 + \bar{H}(\bar{c}_A) \tag{14}$$

$$\frac{\mathrm{d}\varphi}{\mathrm{d}\tau} = -R_1 + I_0 + \bar{H}(\bar{c}_A) \tag{15}$$

$$\frac{\mathrm{d}\sigma}{\mathrm{d}\tau} = \frac{1}{N}\frac{\mathrm{d}N}{\mathrm{d}\tau} - \frac{1}{\varphi}\frac{\mathrm{d}\varphi}{\mathrm{d}\tau} + N\varphi^{-2}\mathrm{e}^{-\sigma}(2I_1 + J_3 - R_2 + \bar{H}(\bar{c}_A)) \tag{16}$$

$$\frac{\mathrm{d}\bar{c}_A}{\mathrm{d}\tau} = -AI_0 - A\bar{H}(\bar{c}_A) - \bar{L}(\bar{c}_A) \tag{17}$$

$$\frac{\mathrm{d}m}{\mathrm{d}\tau} = -ABR_1 + BL(\bar{c}_A) \tag{18}$$

where

$$R_i = \frac{N}{\sqrt{2\pi\sigma}}\int_0^\infty \bar{x}^{i-1}\bar{D}(\bar{x})\exp\left[-\frac{1}{2\sigma}\ln^2\left(\frac{\bar{x}}{\hat{v}}\right)\right]\mathrm{d}\bar{x} \tag{19}$$

$$I_i = \frac{N}{\sqrt{2\pi\sigma}}\int_0^\infty \bar{x}^{i-1}\bar{G}(\bar{x},\bar{c}_A)\exp\left[-\frac{1}{2\sigma}\ln^2\left(\frac{\bar{x}}{\hat{v}}\right)\right]\mathrm{d}\bar{x} \tag{20}$$

$$J_0 = \frac{1}{2\pi\sigma}\int_{-\infty}^{\infty}\int_{-\infty}^{\infty}\bar{B}(\hat{v}\mathrm{e}^p,\hat{v}\mathrm{e}^q)\exp\left(-\frac{p^2+q^2}{2\sigma}\right)\mathrm{d}p\ \mathrm{d}q \tag{21}$$

$$J_2 = \frac{1}{2\pi\sigma}\int_{-\infty}^{\infty}\int_{-\infty}^{\infty}\bar{B}(\hat{v}\mathrm{e}^p,\hat{v}\mathrm{e}^q)\times \exp\left(-\frac{p^2+q^2}{2\sigma}+p+q\right)\mathrm{d}p\ \mathrm{d}q \tag{22}$$

$$J_3 = -\frac{1}{2}NJ_0 + NJ_2\mathrm{e}^{-2\sigma} \tag{23}$$

The rate functions of the elementary processes that proceed simultaneously are, in general, quite complicated, so that analytical evaluation of the above integrals is impossible. These integrals must be evaluated numerically in every time step, in the execution of numerical integration of the system of differential equations. This approach renders the method of moments computationally inconvenient; i.e., the advantage from the reduction of eq 7 to only three ODE's is lost due to the large number of integrals which must be numerically evaluated. On the other hand, if rational approximations (simplifications) for the rate functions exist, allowing the integrals (19)−(22) to be evaluated analytically, the method of moments regains its advantages. The present work is based on this idea.

3. Models of Physicochemical Processes

(i) Nucleation. The classical theory of homogeneous nucleation stipulates the generation of nuclei from molecules (Nylt et al., 1985), but in the case of salt precipitation the prevailing mechanism is likely to involve the direct generation of nuclei from ions according to the theory of Chiang et al. (1988). Although this theory is more complicated than the classical one, it provides qualitatively similar results; additionally, information on the (difficult to estimate) liquid−solid surface energy is still required. Thus, the desirability of selecting such a sophisticated theory for modeling practical problems may be questioned. The fact that

there is only a quantitative difference between the two theories and that the nucleation rate is extremely sensitive to the unknown value of the surface energy tends to favor the selection of the classical theory.

At present there are no means, independent of the nucleation method, to compute the surface energy of solids. The only available independent measurement seems to be for $SrSO_4$ (Sohnel and Garside, 1992). The value of the surface energy of inorganic salts is considered to be in a narrow region around 0.1 N/m according to McCabe and Smith (1967). An extensive review of the experimentally determined values of ó$_{\tilde{a}}$ is presented by Sohnel and Garside (1992). In this review it can be seen that the estimated surface energy of a salt differs from one experimental study to another. Obviously, the literature values of surface energy cannot be trusted for use in the present model.

In practice, *heterogeneous* nucleation usually takes place. For heterogeneous nucleation σ_γ may be replaced by σ_a, which is a function of the condition of the solvent (presence of impurities). The best procedure for the experimental evaluation of σ_a is to employ batch conditions, for a specific fluid medium according to the method described by Sohnel and Garside (1992). This method was used by Kostoglou et al. (1995).

(ii) Particle Growth. Particle size growth results from a combination of various steps in series as described by Chiang and Donohue (1988). They first presented a theory for crystal growth with ions (not molecules) as the elementary species. The use of older but simpler theories is considered preferable for reasons outlined in the case of nucleation. It is assumed that all the phenomena occurring on the particle surface during crystal growth can be lumped into the expression of the polynuclear particle growth as given by Nielsen (1984). The diffusive flux of ions toward the particle is given by the solution of diffusion equation in spherical coordinates under pseudo-steady-state conditions (Nielsen, 1960). It can be shown that the assumption of pseudo-steady-state conditions is valid for precipitation of sparingly solube salts. The ionic flux is given as

$$J_i = \frac{D_i(c_i - c_{is})}{R} \qquad i = \text{A, B} \tag{24}$$

where D_i is the diffusion coefficient of the ions, R is the particle radius, and the index s designates the interface concentration.

The fluxes of the two ionic species A and B toward the particle surface must satisfy stoichiometry

$$\frac{J_A}{a} = \frac{J_B}{b} \Rightarrow \frac{D_A}{a}(c_A - c_{As}) = \frac{D_B}{b}(c_B - c_{Bs}) \tag{25}$$

In this equation it is assumed that the role of convection is negligible for mass transfer to the particle. The inclusion of the convective contribution in eq 25 is trivial using the appropriate mass transfer coefficients (computed by the Armenante and Kirwan (1989) correlation, for example). However, the particle sizes in precipitation are usually so small that particles follow exactly the fluid motion and the slip velocity between the particle and fluid is practically zero (Friedlander, 1957). For this reason it is better to avoid useless computations associated with particle/fluid convective transfer.

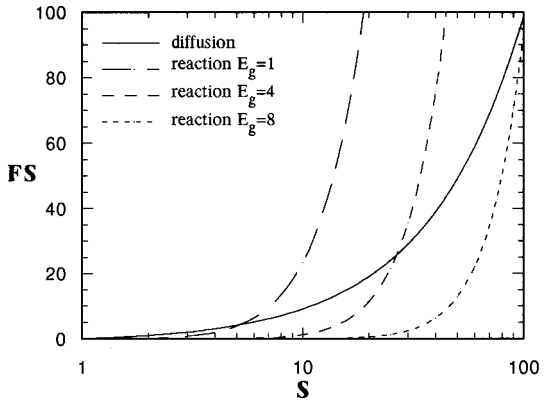

Figure 2. Dimensionless particle growth rate dependence FS on the saturation ratio for diffusion and for surface reaction.

The rate of consumption of ionic species A by surface reaction is

$$J_R = \frac{ak_g}{V_m}(S_s - 1)^{2/3} S_s^{7/6} (\ln S_s)^{1/6} \exp\left(-\frac{E_g}{\ln S_s}\right) \tag{26}$$

where S_s is the saturation ratio at the particle surface.

Putting $J_A = J_R$ and using eq 10, a system of two equations with two unknowns (c_{As} and c_{Bs}) is obtained. The dependence of particle volume on particle growth rate is complicated because the dependences of the elementary mechanisms are different. In this case the analytical evaluation of integral (20) is not possible. However, if one of the two mechanisms dominates, integration can be carried out analytically. Dimensionless growth rate dependences FS (FS $= J_R V_m/ak_g$ for surface reaction controlled growth and FS $= J_A c_{As} R/D_A$ for diffusion controlled growth) on the saturation ratio for diffusion and for surface reaction are shown in Figure 2 for several values of dimensionless energy E_g. Only in a small region of the saturation ratio are the two rates comparable; thus, it is logical to consider that the slower of the two mechanisms dominates the growth process.

For the case where diffusion is the dominant step, the surface concentrations are such that $S_s = 1$ and the following relation is valid:

$$K_{sp} = c_{As}^{\ a} c_{Bs}^{\ b}$$

Combining the above equation with eqs 10 and 25 leads to

$$\frac{aD_B}{bD_A}\left(c_{B0} - \frac{b}{a}c_{A0}\right) + \left(\frac{D_B}{D_A} - 1\right)c_A - \frac{aD_B}{bD_A}\frac{K_{sp}^{\ 1/b}}{c_{As}^{\ a/b}} + c_{As} = 0 \tag{27}$$

This equation is solved for c_{As}, and the growth rate is evaluated from the relation

$$G_d(x,c_A) = (4\pi)^{2/3}(3)^{1/3} V_m \frac{D_A}{a}(c_A - c_{As})x^{1/3} \tag{28}$$

It can be shown that the difference between diffusivities of the two species affects the growth rate, a fact that usually is not taken into account in practical calculations.

If surface reaction is the dominant step, surface concentrations are equal to bulk concentrations so that $S_s = S$. The particle growth rate will be

$$G_r(x,c_A) = (36\pi)^{1/3} k_g (S-1)^{2/3} S^{7/6} (\ln S)^{1/6} \times \exp\left(-\frac{E_g}{\ln S}\right) x^{2/3} \quad (29)$$

In the present model the two growth rates are computed in each time step and the smaller is assumed to be the actual particle growth rate. The reference particle size for evaluating the growth rates is $x = \hat{v}$, since it represents the median size of the distribution. The validity of this assumption tends to improve as the dispersivity of the distribution is reduced. A sharp change between the growth mechanisms, as the saturation ratio is increased, is physically inadmissible, and furthermore creates computational difficulties. To avoid this problem, the following interpolation formula for the growth rate is used if the ratio of the two individual rates is between 0.1 and 10. Of course, this formula must be such that the integral (20) is analytically integrable; i.e.

$$G = \left(\frac{1}{G_d} + \frac{1}{G_r}\right)^{-1} x^{((1/3G_d)+(2/3G_r))((1/G_d)+(1/G_r))^{-1}} \quad (30)$$

The above problem of formulating the appropriate moment equations for the entire particle size spectrum, if different growth mechanisms are operative in different particle size regions, is also encountered in the simulation of aerosol evolution. Small aerosol particles are in the free molecule regime and large particles in the continuum size regime. The growth rate dependence on particle size is different in each regime. Pratsinis (1988) tackled this problem using an entirely different approach from that employed here; he wrote down separate moment equations for each of the two growth mechanisms and obtained the final moment equations by taking the harmonic average of the growth terms that correspond to the two mechanisms. On the other hand, in the present work, the median size of the distribution is employed to determine the dominant mechanism. The accommodation of the approach by Pratsinis (1988) to the present model is straightforward; however, extensive comparisons of the two approaches with exact solutions should be made to establish which one is preferable, under various conditions.

(iii) Ionic Deposition. The diffusive fluxes of ions toward pipe walls are obtained from the relations

$$J_i = k_{mi}(c_i - c_{is}) \qquad i = \text{A, B} \quad (31)$$

where $k_{mi} = 0.07u^* Sc^{-2/3}$ is the mass-transfer coefficient for turbulent convective transport. The rate of ion consumption due to surface reaction at the wall is (Nielsen, 1984)

$$J_r = \frac{a k_d}{V_m} (S_s - 1)^{2/3} S_s^{7/6} (\ln S_s)^{1/6} \exp\left(-\frac{E_d}{\ln S_s}\right) \quad (32)$$

In this case, unlike the case of particle growth, a direct combination of the two mechanisms is possible, as there are no restrictions on the complexity of the relation for deposition rate. Putting $J_A/a = J_B/b = J_r/a$, one obtains

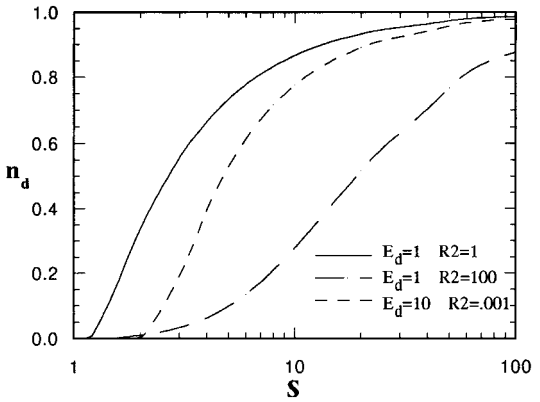

Figure 3. Effectiveness factor n_d for ionic deposition versus saturation ratio for several values of activation energy and ratio R2.

$$\frac{k_{mA}}{k_d}(c_A - c_{As}) - \frac{k_d}{V_m}(S_s - 1)^{2/3} S_s^{7/6} (\ln S_s)^{1/6} \times \exp\left(-\frac{E_d}{\ln S_s}\right) = 0 \quad (33)$$

$$c_{Bs} = c_{B0} - \frac{b}{a}(c_{A0} - c_A) - \frac{b}{a}\left(\frac{D_A}{D_B}\right)^{2/3}(c_A - c_{As})$$

This equation is solved for the interface concentration c_{As}, which allows one to evaluate the deposition rate

$$L(c_A) = k_{mA}(c_A - c_{As}) \quad (34)$$

According to Garside (1971), an effectiveness factor may be defined as

$$n_d = \frac{S - S_s}{S - 1} \quad (35)$$

This factor tends to unity as turbulent diffusion dominates. Figure 3 shows the effectiveness factor versus saturation ratio for several combinations of E_d and of $R2 = k_{mA}/k_d$ (assuming $c_{A0} = c_{B0}$, $a = b = 1$, $D_A = D_B$). Generally, the factor n_d tends faster to unity as E_d and k_{mA}/k_d are increased.

(iv) Coagulation. The main assumption of this work in regards to coagulation is that the two mechanisms of Brownian and turbulent coagulation are independent of each other, and additionally interparticle interactions independently influence each of them. In the absence of interparticle interactions, the above assumption of the additivity of coagulation rates is evaluated in detail by Williams and Loyalka (1991). The error from this assumption is considered acceptable for the present simulation. The additivity principle is extended to the case when interparticle interactions are present:

$$B(x,y) = B_{Br}(x,y) + B_T(x,y) = \frac{2kT}{3\mu W_{Br}(x,y)}\left[2 + \left(\frac{x}{y}\right)^{1/3} + \left(\frac{y}{x}\right)^{1/3}\right] + \frac{3c}{4\pi W_T(x,y)}(x^{1/3} + y^{1/3})\left(\frac{\epsilon_d}{\nu}\right)^{1/2} \quad (36)$$

where the individual coagulation rates are taken from Friedlander (1977). The quantity ϵ_d is the energy dissipation rate which for pipe flow is given as

$$\epsilon_d = \frac{4}{d_t}\left(\frac{f}{2}\right)^{3/2} u^3 \tag{37}$$

Several values have been proposed for the coefficient c in eq 36. According to Saffman and Turner (1956), $c = 1.3$; Yuu (1984) argues that $c = 1.67$; and Delichatsios (1980) gives $c = 0.81$. For the present work the value $c = 1.3$ is selected.

The integrals (21) and (22) must be computed numerically due to the complicated form of the coagulation rate (36), which renders the moment method computationally intractable. It can be shown that as the dispersivity σ of the particle size distribution is decreased, the contribution of the coagulation of particles of size $\hat{v}$ to the integrals is increased. In general, in precipitation processes the dispersivity of the particle size distribution is small so that the main contribution to the integrals (21) and (22) comes from the coagulation between particles of volume $\hat{v}$. When we take this fact into account, it is a good approximation to replace $W(x,y)$ with $W(\hat{v},\hat{v})$ in these integrals. With this replacement the integration can be made analytically. An additional advantage of the above approximation is that it requires the evaluation of the stability ratio only for equal-sized particles, thus avoiding problems related to the computation of double-layer interactions between unequal-sized particles.

The stability ratios for the coagulation between two equal-sized particles of radius R are given as

$$W_{Br} = 2\int_0^\infty \frac{G_p(s)}{(2+s)^2} \exp\left(\frac{\Phi(s)}{kT}\right) ds \tag{38}$$

$$W_T = 24\int_0^\infty \frac{1}{(2+s)^4(1-A(s))} \times \exp\left(\frac{\int_s^\infty \frac{2D_p}{D_T(1-A(s))G_p(s)} \frac{d\Phi(z)}{dz}}{kT}\right) ds \tag{39}$$

where s (made dimensionless with R) is the minimum distance between particle surfaces. D_p is the Brownian particle diffusivity and D_T is the pair diffusivity of particles due to turbulent shear as given by Levich (1962). The function $G_p(s)$ represents the hydrodynamic interaction between two particles moving along their centerline and may be obtained from the solution of Stokes equations in bispherical coordinates. This function is given by Spielman (1970) in series form; however, for extensive computations, the following simple approximate relation given by Honig et al. (1971) is preferable

$$G_p(s) = \frac{6s^2 + 13s + 2}{6s^2 + 4s} \tag{40}$$

The function $A(s)$ in eq 39 also represents hydrodynamic interaction for the motion of two equal-sized spheres, along the line connecting their centers, in shear flow (Russel et al., 1989). The extension of the turbulent diffusion approach to the coagulation in the presence of interparticle forces was recently reported by Gruy and Saint-Raymond (1997), but its validity is questionable because of the use of function $G_p(s)$ in place of $1/(1 - A(s))$. This modification is made in eq 39.

The function $\Phi(s)$ stands for the interaction potential between the particles. This potential is the outcome of two types of forces; attractive van der Waals forces and repulsive (for similarly charged particles) electrical double-layer forces, $\Phi = \Phi_{VdW} + \Phi_{dl}$. The unretarded van der Waals interaction potential is estimated (Israelachvili, 1985) from

$$\Phi_A(s) = -\frac{H_A}{6}\left[\frac{2}{s^2+2s} + \frac{2}{(s+2)^2} + \ln\left(\frac{s^2+2s}{(s+2)^2}\right)\right] \tag{41}$$

where H_A is the Hamaker constant which is characteristic of the specific physicochemical system. As is well-known, the exact computation of the double-layer forces is very complicated even for equal-sized particles. Of all possible conditions at the particle surface, that of constant surface potential is selected for this work. The modification to include other surface conditions is straightforward. The problem of the interaction between two equal particles with constant and small surface potentials has been solved by Glendinning and Russel (1983) with multipole expansion techniques. However, this solution is impractical for extensive computations; for this reason it is preferable to use the two asymptotic relations for the forces as $\kappa R \to 0$ and $\kappa R \to \infty$ where κ is the inverse double-layer thickness which is proportional to the square root of the ionic strength I of the solution.

For particles characterized by $\kappa R > 1$, the method of Derjaguin (exact in the limit $\kappa R \gg 1$) gives (Hogg et al., 1966)

$$\Phi_{dl} = 2\pi\epsilon R\psi_0^2 \ln(1 + e^{-\kappa R s}) \tag{42}$$

Extensive comparisons between this approximate relation and the exact solution are made by Glendinning and Russel (1983), showing that the approximate relation is satisfactory even for $\kappa R < 10$. Recently, Sader et al. (1995) found that if the right-hand side of eq 42 is multiplied by $(1 + s/2)^{-1}$ the results are even better. The solution for the case $\kappa R < 1$ is given by Verwey and Overbeek (1948) using multipole expansion combined with the method of moments (type of weighted residuals method). The final result with second-order expansion (exact in the limit $\kappa R \ll 1$) is

$$\Phi_{dl} = 2\pi\epsilon R\psi_0^2 \frac{e^{-\kappa R s}}{s+2}\left(\frac{1}{1+\mathbf{a}} + e^{-\kappa R s}(1 - e^{-2\kappa R})\frac{1}{2\kappa R(s+2)}\right)^{-1} \tag{43}$$

The relation for **a** is lengthy and can be found elsewhere (Kostoglou and Karabelas, 1991). Thus, to estimate the stability ratio, the potential of double-layer interactions is calculated using eq 42 for $\kappa R > 1$ and using eq 43 for $\kappa R < 1$. There is no simplified theory for determining the interaction of two unequal particles characterized by $\kappa R > 1$ for one size and by $\kappa R < 1$ for the other. However, this problem is avoided because only the stability ratio for coagulation between equal-sized particles is required in the model proposed in this work.

(v) Particulate Deposition. The paricle flux to the pipe surface for monodisperse particles can be written as

$$J = k_p N \tag{44}$$

Available expressions (e.g., Papavergos and Hedley, 1984) can be used to compute the transfer coefficient

k_p. Using a differential mass balance, one obtains the rate expression

$$D(x) = \frac{4}{d_t} k_p \tag{45}$$

The expression for k_p, applicable to very small particles, must be extended to include particle/wall interactions. One approach is by solving the diffusion equation for turbulent pipe flow (Williams and Loyalka, 1991) with a particle/wall energy barrier and hydrodynamic interactions. The final result for the deposition rate is

$$D(x) = \frac{4}{d_t} \frac{0.042u^*}{W_d(x)} \left(\frac{kT\rho_f}{6\pi\mu^2}\right)^{2/3} x^{-2/9} \tag{46}$$

where

$$W_d(x) = 1 + \frac{d_t D(x)}{D_p} \int_0^\delta \left[G_d(s) \exp\left(\frac{\Phi_d}{kT}\right) - 1 \right] ds \tag{47}$$

D_p is the diffusivity of a particle with volume x. The distance δ is selected such that the particle/wall force is negligible at that distance. The function $G_d(s)$ represents the hydrodynamic particle/wall interaction given in a series form by Brenner (1961). A convenient approximate relation for this work is given in Appendix II:

$$G_d(s) = 1 + \frac{1}{s} + \frac{0.128}{s^{0.5}} \tag{48}$$

The interaction potential is comprised again of two parts: $\Phi_d = \Phi_{dVdW} + \Phi_{ddl}$. The van der Waals potential for the particle/wall interaction is (Israelachvili, 1985)

$$\Phi_{dVdW} = -\frac{H_{Ad}}{6} \left(\frac{2(s+1)}{s(s+2)} - \ln\left(\frac{s+2}{s}\right) \right) \tag{49}$$

The new Hamaker constant H_{Ad} depends additionally on the wall material. As regards the double-layer interaction potential, the Derjaguin method is used for $\kappa R > 1$. The perfomance of this method is even better than that in the case of two particles because here one of the surfaces has zero curvature. If ψ_1 is the wall surface potential, the double-layer interaction potential is given by the relation

$$\Phi_{ddl} = 2\pi\epsilon R[(\psi_0 + \psi_1)^2 \log(1 + e^{-\kappa R s}) + (\psi_0 - \psi_1)^2 \log(1 - e^{-\kappa R s})]$$

Although in recent years sophisticated numerical techniques (singularities method (Phillips, 1995); boundary element method (Grant and Saville, 1995)) or approximating methods (method of images (Nitsche, 1996)) have been used for the computation of particle/wall double-layer interactions, there is no simple relation (to the best of our knowledge) for the particle/wall interactions for the case $\kappa R < 1$ and arbitrary particle/wall distance. To fill this gap, a weighted residuals moment method is used here, similar to that of Verwey and Overbeek for the case of two spheres. The results for two spheres show that even the first-order approximation is sufficient for $\kappa R < 1$. The details of this effort and the final expression are not shown here because, although relatively simple, they are lengthy.

4. Numerical Implementation

The guidelines for developing a numerical scheme, to solve the above problem, are to minimize the probability of failure (under various physicochemical conditions) and to maximize computational efficiency. The system of ODE's (14)−(18) is stiff. An integration method for stiff systems is used, based on the implicit Runge−Kutta method of third order, with a self-adjusted step and prespecified accuracy (Villadsen and Michelsen, 1978). Even with this method, a few hundred integration steps are required for an acceptable accuracy. For this reason the reduction of computations in a single integration step is crucial for overall efficiency. Thus, analytical evaluation of the required Jacobian (wherever possible), although cumbersome, is important for improving the efficiency of the code. Numerical overflow problems related to the very fast process of nucleation must be dealt with carefully. The usual way is to use the logarithms of the variables in the computations.

Numerical evaluation of integrals (38) and (39) is difficult because the integrand can be very steep. The best way to proceed is with their transformation to differential equations. Integration of the resulting differential equations is carried out with an explicit fourth-order Runge−Kutta method with a self-adjusted step and prespecified accuracy (Press et al., 1986). A few decades of steps are required for this integration. Evaluation of the stability ratio in every time step can reduce considerably the efficiency of the technique. It is noted, however, that the stability ratio for a particular physicochemical system depends only on particle volume. Thus, it is very advantageous to compute in advance the stability ratio W for certain values of the particle volume and subsequently to determine W in each time step by interpolation (considering that only the particle volume changes with time). Particle volumes at which the stability ratio is precomputed are $x_i = 2^i\alpha$ ($i = 0, 1, 2, ...$); i.e., they represent the center of classes typically used in sectional methods for the solution of population balances. The best interpolation method is the piecewise linear interpolation of $\ln(W)$ versus particle radius R. It is in agreement with the suggestion of Bogush and Zukoski (1991) that the stability ratio is a power function of the particle radius. An approximate method also exists for the computation of the stability ratio when the integrand has a maximum (Kostoglou and Karabelas, 1991) but the computational benefit of its use is too small to compensate for the loss of accuracy.

The transcendental equations (27) and (33) must be solved numerically. The advantage from the preevaluation of growth and deposition rates is not comparable to that for the stability ratio, because the computation of these rates is relatively easy and depends on two variables that change in the integration; i.e., particle size and active species concentration. Identifying the best method for the solution of eqs 27 and 33 is not a trivial matter. The form of the equations is such that the Newton−Raphson method usually diverges and leads to code failure. On the other hand, the bisection method converges safely but is very inefficient computationally. It appears that the best choice is the Van Wijngaarden−Dekker−Brent method (Press et al., 1986) that combines the merits of the above methods; i.e., it

Table 1. Parameter Values Used in Computer Simulations

T, K	498	k_g, m/s	0.1
d_t, m	0.127	k_d, m/s	10
τ_0, s	2000	E_d	10
u, m/s	0.5	E_g	1
c_{A0}, grion/L	10^{-5}	σ_a, N/m	0.08
c_{B0}, grion/L	10^{-5}		

ensures convergence, and it is much faster than the bisection method.

5. Results

As the model considered here has a large number of parameters, its complete parametric study is beyond the scope of the present publication. Instead, a set of typical conditions are selected, and the effect of some key parameters, of special interest, are adequately studied. It is assumed that the physicochemical data (V_m, MB, a, b, d_A, d_B, ρ) of the active species are those of PbS. The features of the flow system (τ_0, u, d_t, T, P) are considered to be typical of a geothermal plant. Indicative values of the constants of crystallization and nucleation (σ_a, k_g, k_d, E_g, E_d) are selected. In Table 1 the values of these parameters are summarized. Inlet concentrations of PbS in the real installations are between 2 and a few decades of ppm (Andritsos and Karabelas, 1991a). Since this concentration cannot be controlled, it is a fixed variable for the model; for the purpose of demonstration, a relatively low value ($c_A = c_B = 10^{-5}$ grion/L) is selected. The manipulated (or controlled) variable in order to reduce the fouling rate is the initial saturation ratio (S_0), which in practice can be adjusted with the appropriate control of pH. Therefore, S_0 is a key parameter to be studied here. Two values are selected, a relatively small one ($S_0 = 3$) and a relatively large one ($S_0 = 10$). These values are chosen after extensive trials in order to cover the two different regions of the system behavior as will be shown below. The second parameter to be studied is aimed at assessing the models employed and not merely the influence of a specific variable; thus, the effect of the stability ratio W on the model results is examined. Since W depends on several system variables, it will be convenient to study only the two extreme cases of *no coagulation* ($W = \infty$) and *uninhibited coagulation* ($W = 1$). If the results of these two cases are close to each other, it means that the use of the exact stability ratio can be avoided. In the opposite case, the stability ratio must be used in its exact form.

The results for four different cases are displayed and analyzed. These cases are obtained by combining the above two initial supersaturations with the two extremes of uninhibited and no coagulation. Figure 4 shows the total particle number concentration along the pipe. It is worth noting that the particle size distribution in the case of no coagulation is monodisperse ($\sigma = 0$). This means that the nucleation is very fast compared to particle growth so that the two phenomena proceed independently in time. In this case only coagulation can broaden the distribution. For $S_0 = 10$ the large initial particle number (of order 10^{14}/cm^3) is reduced exponentially along the pipeline. This is expected because, for a monodispersed particle distribution, the rate of particulate deposition is proportional to the total particle number concentration. In the case of uninhibited coagulation ($W = 1$), the total number concentration is sharply reduced to a value of 10^9/cm^3

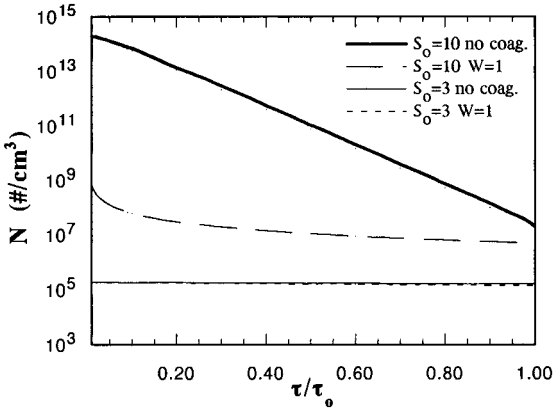

Figure 4. Particle number concentration along the flow path.

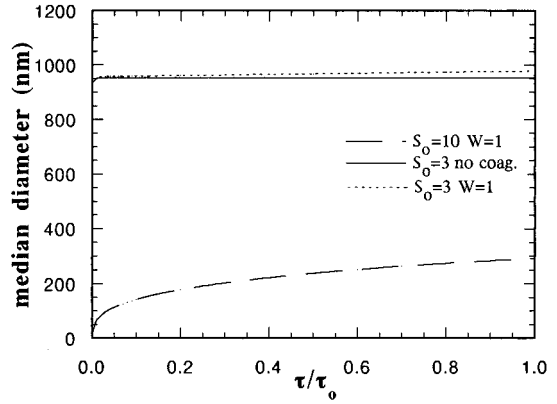

Figure 5. Diameter corresponding to the logarithmic mean volume of the particles along the flow path.

in the first 10 m of the pipe. For these small particle sizes, coagulation is purely Brownian, so that the coagulation rate is proportional to the square of the total particle number concentration. Therefore, one can explain the large initial rate of coagulation for $S_0 = 10$, $W = 1$. For longer lengths of pipe, the reduced total number concentration leads to smaller coagulation rates. It is interesting to note that in this case there is practically no loss of particles due to particulate deposition as in the case of no coagulation. This can be attributed to the larger size of particles (due to coagulation) and to the dependence $x^{-2/9}$ of the particulate deposition rate on the particle volume. For a low initial saturation ratio ($S_0 = 3$) the nucleation rate is small and the total particle number is also small (10^5/cm^3); thus, coagulation proceeds very slowly and its influence on the total particle number is insignificant. Consequently, the difference of the total particle number between the cases of uninhibited and no coagulation is very small (the maximum difference is nearly 15% at the exit of the pipe).

The evolution of the median diameter of the distribution (based on median particle volume) along the pipe is shown in Figure 5. The median diameter is practically equal to the arithmetic mean, except in the case of $S_0 = 10$ with uninhibited coagulation, where it is approximately 12% smaller. For $S_0 = 10$ the nucleation is very fast and produces a large number of particles. The major part of the active species is consumed through nucleation, while the remaining ions are insufficient to cause significant growth to the huge number of nuclei already formed. After a short period of particle growth, the particles have a diameter of approximately 1 nm. If there is no coagulation, this is the final particle

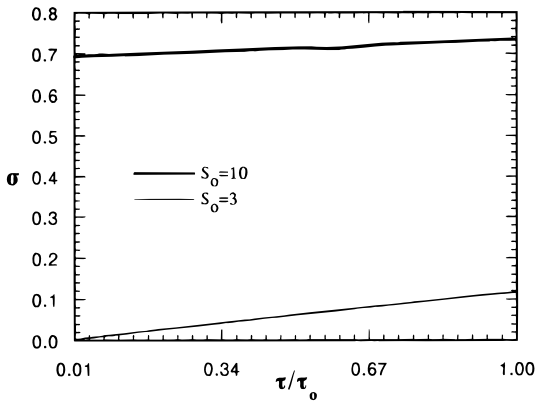

Figure 6. Dispersivity of the particle size distribution along the flow path for uninhibited coagulation ($W = 1$).

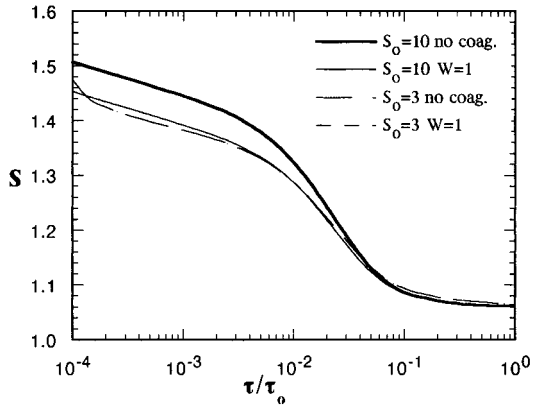

Figure 7. Variation of the saturation ratio along the flow path.

size, but for uninhibited coagulation the size of the particles increases along the pipe, as is shown in Figure 5. For $S_0 = 3$ the number of initially produced nuclei is small; so, there exists enough active material for further particle growth. The latter proceeds very fast and leads to relatively large particles (of order 1 μm diameter). If there is no coagulation, this size is constant along the rest of the pipe. For the case of uninhibited coagulation there exists a gradual increase of the particle diameter (approximately 3% at the pipe exit).

Figure 6 displays the dispersivity σ of the particle size distribution. As stated already, for the case of no coagulation the dispersivity is zero (monodispersed distribution). For $S_0 = 10$ with coagulation, Brownian coagulation takes place very fast and the distribution acquires its self-similar form with $\sigma = \log(2)$. Thereafter, turbulent coagulation begins to be effective, causing a small but steady increase of the dispersivity. The exit value of the dispersivity is 0.734. For $S_0 = 3$, coagulation proceeds very slowly and leads to an almost linear increase of the dispersivity along the pipe with exit value $\sigma = 0.12$.

Figure 7 shows the evolution of the saturation ratio along the flow path. The scale is logarithmic to magnify some points relevant to particle growth which are impossible to discern with a linear scale. It is pointed out that, after a very short entrance pipe length, the only phenomenon that can influence the saturation ratio is the ionic deposition on the pipe walls. Indeed, in the pipe length between approximately 10 cm and 10 m (as shown in Figure 7) the nucleation and the diffusional particle growth are terminated, and the slope of the saturation ratio curves is affected mainly by a surface-

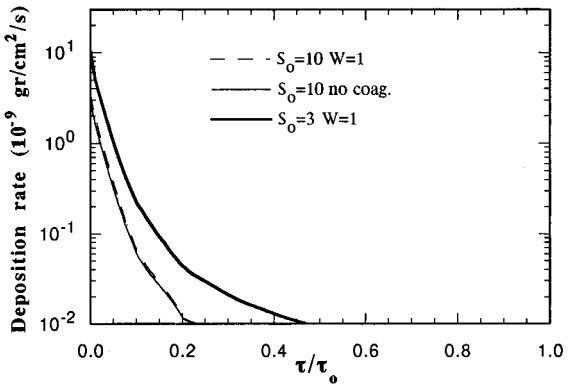

Figure 8. Ionic deposition rate along the flow path.

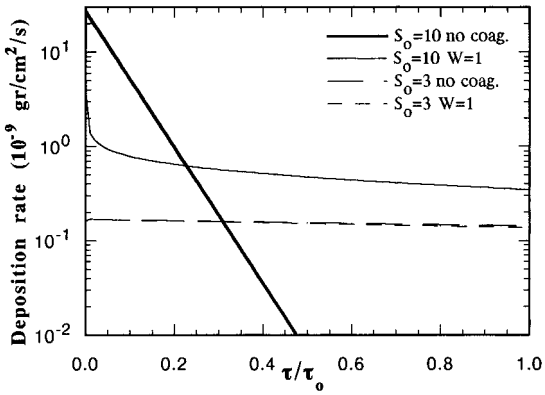

Figure 9. Particulate deposition rate along the flow path.

reaction type particle growth. The latter becomes also unimportant before the tenth meter of the pipe; beyond that, the slope of the saturation ratio is affected by ionic deposition on the wall due to turbulent convective diffusion. The final small slope is due to surface reaction controlled ionic wall deposition. The difference of saturation ratio curves between the cases of uninhibited and no coagulation for $S_0 = 10$ is due to the large extent of coagulation for this value of the saturation ratio. On the contrary, for $S_0 = 3$ the extent of coagulation is so small that the difference between the cases of $W = 1$ and $W = \infty$ is negligible. Actually the two curves in Figure 7 are indistinguishable. The very large initial slope that appears for $S_0 = 3$ corresponds to the final stages of the diffusional particle growth.

The most interesting results of the present study, from the practical point of view, are related to the deposition rate. There exist two kinds of deposition: *ionic* and *particulate*. Considering the same amount of deposits of the two kinds, the particulate deposit is less problematic in industrial installations because it has a loose structure that renders easier its removal by the flow. Because of their different features, the two kinds of deposition will be analyzed separately. Figure 8 presents the ionic deposition rate versus pipe length. In all cases this deposition rate is a monotonically decreasing function of the length along the pipe. For large supersaturations a difference of approximately 15% exists between the cases of uninhibited and no coagulation, with the case of no coagulation associated with larger deposition rates. For small supersaturations the deposition rate is indistinguishable between the two cases of the coagulation rate. The corresponding particulate deposition rate is shown in Figure 9. The results in this figure could be anticipated because for

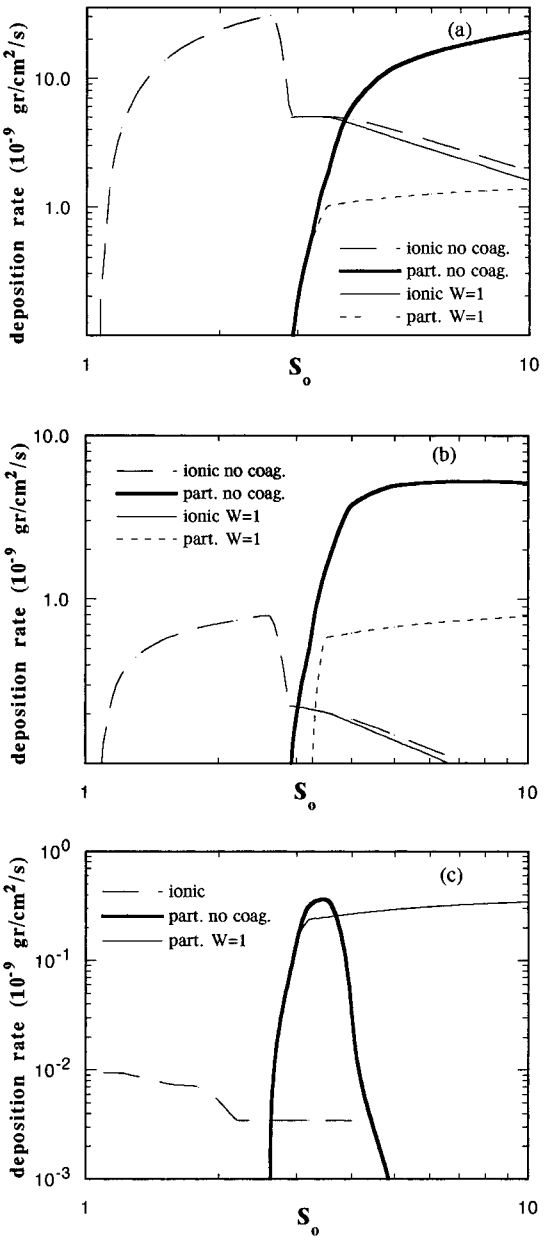

Figure 10. Ionic and particulate deposition rates versus initial saturation ratio at three distances along the pipe: (a) 10 m, (b) 100 m, (c) exit of the pipe.

small dispersivity the deposition rate is almost proportional to the local total particle number concentration. Thus, the curves of this figure are very similar to those of Figure 4. It is noteworthy that for large supersaturations the process of coagulation can modify considerably the particulate deposition rate.

Figure 10 presents perhaps the most interesting results of this example. The particulate and ionic deposition rates for the cases of uninhibited and no coagulation are plotted versus initial saturation ratio, at three locations of the pipeline in parts a−c of Figure 10. The first location is near the entrance of the pipe (10 m), the second at a distance of 100 m, and the third at the pipe exit. It must be pointed out that the *critical* saturation ratio (Kostoglou et al., 1995) for the system under consideration is $S_c = 2.6$. As can be seen in Figure 10a, the ionic deposition starts at small values of the saturation ratio and tends to sharply increase with increasing the initial saturation ratio. A maximum followed by a steep reduction of the deposition rate

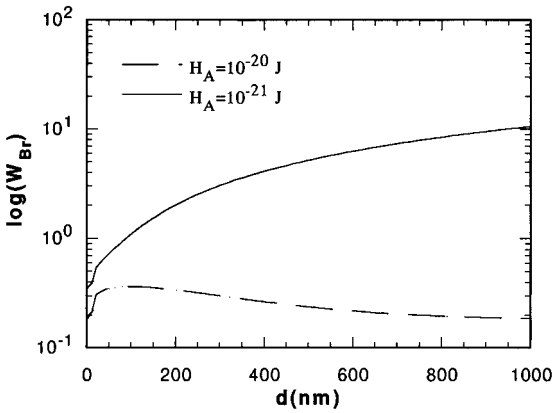

Figure 11. Brownian stability ratio W_{Br} between equal-sized particles, for $\kappa^{-1} = 10$ nm, $\psi_0 = 25$ mV, and two values of the H_A, versus particle diameter d.

appears around the value S_c. For larger supersaturations the deposition rate tends to decrease smoothly. The case of no coagulation is associated with a rather small increase of ionic deposition rate only for $S_0 > 3.5$. Particulate deposition appears at $S_0 = S_c$ and tends to sharply increase with the saturation ratio. For large supersaturations it seems to approach an asymptote, for $S_0 > 30$. In the region close to $S_0 = S_c$, coagulation does not influence the particulate deposition rate but for larger saturation ratio, it leads to a drastic reduction, by 1 order of magnitude.

For the location $x = 100$ m, the behavior of the deposition rates is the same as that for $x = 10$ m, but their absolute values are an order of magnitude smaller, as can be seen in Figure 10b. The particulate deposition rates attain their asymptotic values at lower supersaturations. The process of coagulation restricts particulate deposition to the region $S_0 > 3.2$. At the pipe exit (Figure 10c) ionic deposition is negligible. In the case of uninhibited coagulation, particulate deposition appears at $S_0 = S_c$; beyond this point it increases sharply and finally remains nearly constant for large supersaturations. If there is no coagulation, the particulate deposition rate exhibits a maximum followed by a steep decrease to a zero value at $S_0 \approx 5$. This behavior is due to the fact that if no coagulation takes place, the particles tend to be deposited on the pipe walls before they arrive at the pipe exit. From the above results it becomes clear that coagulation has a rather small influence for supersaturations near the critical one and for ionic deposition, but it is very significant for large supersaturations and for particulate deposition. For this reason the coagulation process must be taken into account (as accurately as possible) using the stability ratio.

To compute the stability ratio for coagulation, three new parameters are required: Hamaker constant H_A, particle surface potential ψ_0, and the inverse double-layer thickness κ. For the stability ratio relating to deposition, two additional parameters are needed: particle/wall Hamaker constant H_{Ad} and wall potential ψ_1. To better understand the behavior of the stability ratio, some representative values will be given as functions of particle size. The parameter values considered are $\psi_0 = 25$ mV, $\kappa^{-1} = 10$ nm, and two extreme values for the Hamaker constant, a small one (10^{-21} J) and a large (10^{-20} J) one. The Brownian stability ratio W_{Br} is plotted versus the particle diameter in Figure 11. Generally for particles of the size order of a nucleus,

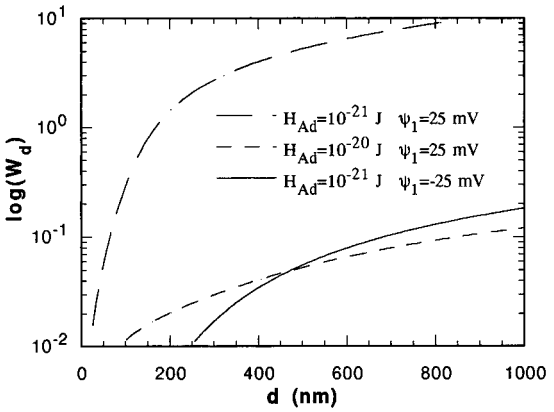

Figure 12. Stability ratio W_d for deposition, for $\kappa^{-1} = 10$ nm, $\psi_0 = 25$ mV, and several values for H_{Ad} and ψ_1, versus particle diameter d.

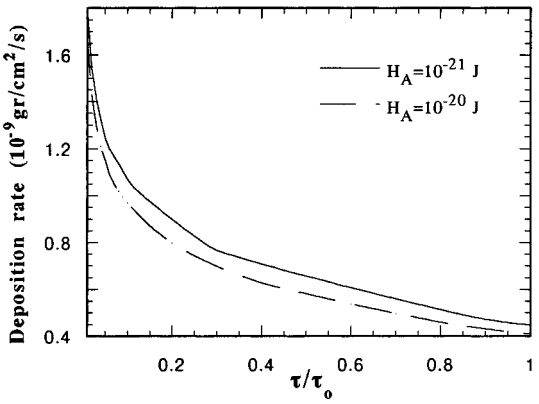

Figure 13. Particulate deposition rates along the flow path for slow coagulation ($\kappa^{-1} = 10$ nm, $\psi_0 = 25$ mV, and two values of H_A).

the stability ratio is on the order of unity. Two types of behavior of the stability ratio are identified with increasing particle size. In the first case ($H_A = 10^{-20}$ J, *fast coagulation*) the curve of the stability ratio versus particle size exhibits a maximum followed by a gradual reduction, with W_{Br} remaining of order unity. In this case the use of the stability ratio has a very small effect on the results. In the second case ($H_A = 10^{-21}$ J, *slow coagulation*) the stability ratio increases sharply and, above a certain particle size, coagulation practically stops. It must be pointed out, however, that coagulation does not totally vanish for very small particles (e.g., close to nuclei size) for which the stability ratio takes small values. This is also consistent with recent results from Zukoski et al. (1996), who argue that other classical DLVO forces (e.g., solvation structural forces) may play a dominant role in the stability of very small particles. For constant ψ_0 and κ the transition from the first case to the second case takes place as H_A is reduced, as can be seen in Figure 11. Figure 12 is similar to Figure 11 but refers to the particle/wall stability ratio W_d. There are also two cases of fast and slow deposition. When ψ_1 is relatively small or of opposite sign compared to ψ_0, then the deposition is fast and neglecting W_d would not modify considerably the results. For the other case of slow deposition, W_d increases as the particle size increases and particulate deposition practically stops above a certain size. For the case of fast deposition the model results are the same as those previously given (Figures 4−10). For the case of slow deposition, the only difference is related to the rate of particulate deposition which is zero for $S_0 = 3$ and is restricted to the first sections of the pipe for $S_0 = 10$ with coagulation.

In practical cases additional interrelations between parameters may exist. For example, ψ_0 and ψ_1 are usually functions of pH (see Adomeit and Renz, 1996). If pH is used as the means for adjusting the saturation ratio, these dependencies must be taken into account. Also, large electrolyte concentrations (up to 20% in geothermal fluids) are not unusual, causing problems in the evaluation of interparticle forces. In this case, the Poisson−Boltzmann equation is not valid and the electric double layer may be studied with the methods of statistical thermodynamics (Tang et al., 1990). As there is no simple theory for the interparticle forces in large electrolyte concentrations, it is rational (as a first approximation) to extend the relevant theory used for dilute electrolyte solutions.

The effect of the coagulation stability ratio on the model results is further discussed here and contrasted with the extremes $W = 1$ and $W = \infty$. First, the case of small saturation ratio, $S_0 = 3$, is considered. If the parameters of the interparticle forces are such that they favor coagulation, the results are very similar to those for uninhibited coagulation ($W = 1$). If the parameter values lead to reduced coagulation (i.e., large stability ratios), the instantaneous growth of particles results in large particle diameters; therefore, the end result is the same as that for the case of no coagulation. Second, the case of relatively large saturation ratio, $S_0 = 10$, is treated. The transition between the cases of fast and slow coagulation is smooth, depending on parameters of interparticle forces. Typical results, in support of the above trends, are obtained for $\kappa^{-1} = 10$ nm, $\psi_0 = 25$ mV, and two values of H_A, a small one (10^{-21} J) and a large one (10^{-20} J). For both values of H_A, the dispersivity of the distribution is very close to that of the self-similar distribution (within 0.5%). The axial variation of the saturation ratio is the same as that in the case of uninhibited coagulation (see Figure 7). Furthermore, ionic deposition is the same except for small differences of order 1% close to the pipe entrance. The particulate deposition rate for the two H_A values is shown in Figure 13. The reduction of the total number concentration resembles that for uninhibited coagulation but is slower as H_A decreases. Also the particle size increases faster as H_A is increased.

In conclusion, for small initial supersaturations the assumption of uninhibited ($W = 1$) and no ($W = \infty$) coagulation holds well for the cases of fast and slow coagulation, respectively. The difference of the results between the two coagulation extremes is rather small (up to 30%). For large initial supersaturations, only the case of uninhibited coagulation is representative of fast coagulation; as the mode of coagulation changes from fast to slow (with change of the relevant parameters of the stability ratio), the results deviate gradually from those of uninhibited coagulation, and in any case are quite different from those of no coagulation.

6. Concluding Remarks

A general methodology has been developed for simulating precipitation phenomena, with emphasis on pipe wall fouling, in turbulent flow. The required computer code is optimized in regards to speed of execution at an accuracy level adequate for practical purposes. The main problem, however, is that for several parameters

no reliable values can be found in the literature. Even the use of some available literature values cannot be made with confidence as they are strongly dependent on the method of determination. It will be noted that the parameters σ_a, ψ_0, and ψ_1 can be measured using procedures independent of the processes included in the present simulation algorithm, i.e., light absorption, electrophoresis, and streaming potential, respectively. However, the rest of the parameters can be found from experiments similar to the simulated processes. Thus, the deposition surface-reaction constants k_d and E_d may be estimated from measurements of deposits in turbulent pipe flow for $1 < S < S_c$ (no bulk precipitation). The Hamaker constants H_A and H_{Ad} may be obtained from experiments in the presence of particles: H_A from particle size measurements of coagulated particles (with photon correlation spectroscopy) and H_{Ad} from deposition rate measurements under turbulent pipe flow. Finally, particle growth surface-reaction constants may be estimated from batch precipitation tests with continuous measurement of active species concentration or of particle size. It will be added that recently Bramley et al. (1996) proposed a method for direct determination of individual process rates from precipitation experiments by employing a simplified population balance approach.

For parameter estimation, subprograms of the present code could be used. A parameter estimation routine requires many calls of the code; therefore, code reliability and speed of execution are essential. With such a code available, it seems highly desirable to apply the above procedure, for several insoluble salts, to create a database of the parameters affecting their precipitation. In practical applications (as is the case with geothermal fluids) several substances are present in the solution. In general, the required calculations of equilibria are quite complicated and an appropriate chemical equilibrium code (e.g., HYDRAQL; Papelis et al., 1988) must be called in every time step to evaluate instantaneous saturation ratios of each substance. Additionally, the model must be extended with the population balance and mass balance for every precipitating substance in the system. This is straightforward for nucleation and particle growth because observations suggest that these processes may proceed independently for each substance (no coprecipitation). However, the possibility of coagulation of particles of different substances is an open question and obviously increases tremendously the complexity of the model. A relevant problem for which an analysis exists is the precipitation of polymorphs (Chakraborty and Bhatia, 1996).

The comprehensive model presented here is subject to improvement as new results become available for elementary mechanisms (e.g., particle detachment, not included here) and their interactions. Along these lines, it should be pointed out that such interactions are currently taken into account only macroscopically through population balance. Indeed, very seldom does one consider interactions at the microscopic scale. For example, nucleation may be affected by particle growth due to the resulting uneven concentration distribution of active species around each particle (Alam and Flagan, 1984). The growth of particles may also lead to an increase of the coagulation rate, since it appears to facilitate particle contact, as deduced from the experimentally obtained dependence of the coagulation rate on the saturation ratio (Bramley et al., 1997). This area is open for future study, despite some work already carried out (Marchal et al., 1991). It will be added here that, on the basis of the test case analyzed in this paper, there are indications that at each instance (or pipe crosssection) one of the processes may take place much faster than the others, suggesting that elementary process interactions may be limited. Much more work is certainly required in all levels to clarify these issues.

Acknowledgment

Grateful acknowledgment is made of financial support from the European Commission under Contract JOU2-CT92-0108.

Appendix A. Particulate Deposition Rate from Turbulent Pipe Flow in the Presence of Particle/Wall Interactions

There are several approaches in the literature to estimate particulate deposition from a turbulent flow in the precence of particle/wall interactions. Models are reported, relying on the structure of turbulence at the wall such as fluid downsweeps and periodically developing boundary layers (Dabros and Van de Ven, 1983), two-dimensional $k-\epsilon$ models (Adomeit and Renz, 1996), and semiempirical correlation of experimental data (Vasak et al., 1995). The use of a phenomenological model, based on the eddy diffusivity concept, is considered adequate for the present study. It is characterized by simplicity (compared to other methods) and compatibility with the relation recommended by Papavergos and Hedley (1984).

The particulate deposition rate can be found from the solution of the convective-diffusion equation for turbulent flow at a specified point of the pipe

$$\frac{\theta}{\theta z}\left[\frac{(D_p+\epsilon)}{G_d}\left(\frac{\theta N}{\theta z}+\frac{ND_p}{kT(D_p+\epsilon)}\frac{d\Phi_d}{dz}\right)\right]=0 \quad \text{(A1)}$$

where ϵ is the eddy diffusivity and z is the distance from the pipe wall. The boundary conditions for the above equation are $N = 0$ at $z = 0$ and $N = N_\infty$ (where N_∞ is the particle concentration at the bulk) for $z = \infty$. After solving the above boundary value problem and evaluating the flux at $z = 0$, the following relation results:

$$J=\left[\int_0^\infty \frac{G_d \exp\left(\frac{1}{kT}\int_z^\infty \frac{d\Phi_d}{ds}\frac{D_p}{D_p+\epsilon}ds\right)}{D_p+\epsilon}dz\right]^{-1} \quad \text{(A2)}$$

If J_F is the deposition rate in the absence of particle/wall interactions ($G_d = 1$, $\Phi_d = 0$), then

$$W_d=\frac{J_F}{J}=\left(\int_0^\infty \frac{1}{D_p+\epsilon}dz\right)^{-1}\int_0^\infty \frac{G_d \exp\left(\frac{1}{kT}\int_z^\infty \frac{d\Phi_d}{ds}\frac{D_p}{D_p+\epsilon}ds\right)}{D_p+\epsilon}dz \quad \text{(A3)}$$

To facilitate the integration at the numerator, it is observed that the interaction potential is significant only in a narrow region near the pipe wall where the eddy diffusivity is negligible and the particles are only subject to Brownian motion. It is equivalent to the interaction

force boundary layer approximation developed by Ruckenstein and Prieve (1973) and Spielman and Friedlander (1974). By taking this into account, the following relation results:

$$W_d = 1 + \frac{J_F}{D_p}\int_0^{\delta}\left(G_d \exp\left(\frac{\Phi_d}{kT}\right) - 1\right) dz \qquad (A4)$$

where at distance δ the interaction potential is negligible. In contrast with the case of deposition from laminar flow (Elimelech et al., 1995), the above relation is valid even in situations where no interparticle energy barriers exist. This is a consequence of the fact that the integral in eq A4 always converges due to the dependence of turbulent diffusivity on the distance from the wall.

Appendix B. Improved Simplified Relation for Particle/Wall Hydrodynamic Interactions

The function $G_d(s)$ is given by Brenner (1961) and results from the solution of Stokes equations in bispherical coordinates. This function has a series form, and its direct use for extensive computations is inconvenient. An approximate expression can be obtained from the relation of Alam (1987) for two spheres if the ratio of their radii is taken equal to infinity. In this case the relation of Alam is simplified as

$$G_d(s) = 1 + 1/s \qquad (B1)$$

(this result has also been given previously by Dahneke (1974)) which is a very poor approximation of the exact solution. To improve it, a term of the form $\underline{c}/s^{0.5}$ is added where the constant $\underline{c}$ is chosen to minimize the integral of the square of the difference between the exact and approximate values in the interval $0.05 < s < 5$. Finally

$$G_d(s) = 1 + 1/s + 0.128/s^{0.5} \qquad (B2)$$

A comparison with the exact values of $G_d(s)$ shows that the new relation (B2) is significantly improved over the Alam relation (B1). For $s > 10$ the asymptotic relation $G_d(s) = (s - 1/8)/(s + 1)$ must be used.

Literature Cited

Adomeit, P.; Renz, U. Deposition of fine particles from a turbulent liquid flow: Experiments and numerical predictions. *Chem. Eng. Sci.* **1996**, *51*, 3491.

Alam, M. K. The effect of van der Waals and viscous forces on aerosol coagulation. *Aerosol Sci. Technol.* **1987**, *6*, 41.

Alam, M. K.; Flagan, R. C. Simultaneous homogeneous nucleation and aerosol growth. *J. Colloid Interface Sci.* **1984**, *97*, 232.

Andritsos, N.; Karabelas, A. J. Sulfide scale formation and control: the case of lead sulfide. *Geothermics* **1991a**, *20*, 343.

Andritsos, N.; Karabelas, A. J. Crystallization and deposit formation of lead sulfide from aqueous solutions. I. Deposition rates. *J. Colloid Interface Sci.* **1991b**, *145*, 158.

Andritsos, N.; Karabelas, A. J. Crystallization and deposit formation of lead sulfide from aqueous solutions. II. Morphology of deposits. *J. Colloid Interface Sci.* **1991c**, *145*, 170.

Armenante, P. M.; Kirwan, D. J. Mass transfer to microparticles in agitated systems. *Chem. Eng. Sci.* **1989**, *44*, 2781.

Barret, J. C.; Jheeta, J. S. Improving the accuracy of the moments method for solving the aerosol general dynamic equation. *J. Aerosol Sci.* **1996**, *27*, 1135.

Bogush, G. H.; Zukoski, C. F. Uniform silica particle precipitation: An aggregative growth model. *J. Colloid Interface Sci.* **1991**, *142*, 19.

Bramley, A.; Hounslow, M.; Ryall, R. L. Aggregation during precipitation from solution: A method for extracting rates from experimental data. *J. Colloid Interface Sci.* **1996**, *183*, 155.

Bramley, A.; Hounslow, M.; Ryall, R. L. Aggregation during precipitation from solution: Kinetics for calcium oxalate monohydrate. *Chem. Eng. Sci.* **1997**, *52*, 747.

Brenner, H. The slow motion of a sphere through a viscous fluid towards a plane surface. *Chem. Eng. Sci.* **1961**, *16*, 242.

Brock, J. Simulation of aerosol dynamics. In *Theory of dispersed multiphase flow*; Meyer, R. E., Ed.; Academic Press: New York, 1983.

Chakraborty, D.; Bhatia, S. K. Formation and aggregation of polymorhs in continuous precipitation. 1. Mathematical modeling. *Ind. Eng. Chem. Res.* **1996**, *35*, 1985.

Chiang, P.; Donohue, M. D. A kinetic approach to crystallization from ionic solution I. Crystal growth. *J. Colloid Interface Sci.* **1988**, *122*, 230.

Chiang, P.; Donohue, M. D.; Katz, J. L. A kinetic approach to crystallization from ionic solution I. Crystal nucleation. *J. Colloid Interface Sci.* **1988**, *122*, 251.

Cohen, E. R.; Vaughan, E. U. Approximate solution of the equations for aerosol agglomeration. *J. Colloid Interface Sci.* **1971**, *35*, 612.

Crundwell, F. K. Micro-mixing in continuous particulate reactors. *Chem. Eng. Sci.* **1994**, *49*, 3887.

Dabros, T.; Van de Ven, T. G. M. On the convective diffusion of fine particles in turbulent flow. *J. Colloid Interface Sci.* **1983**, *92*, 403.

Dahneke, B. Diffusional deposition of particles. *J. Colloid Interface Sci.* **1974**, *48*, 520.

Delichatsios, M. A. Particle coagulation in steady turbulent flows: Application to smoke aging. *J. Colloid Interface. Sci.* **1980**, *78*, 163.

Den Ouden, C. J. J.; Thompson, R. W. Analysis of the formation of monodisperse populations by homogeneous nucleation. *J. Colloid Interface Sci.* **1991**, *143*, 77.

Dirksen, J. A.; Ring, T. A. Fundamentals of crystallization: Kinetic effects on particle size distributions and morphology. *Chem. Eng. Sci.* **1991**, *46*, 2389.

Elimelech, M.; Gregory, J.; Jia, X.; Williams, R. *Particle Deposition & Aggregation: Measurement, Modelling and Simulation*; Butterworth-Heinemann: Oxford, U.K., 1995.

Friedlander, S. K. Behavior of suspended particles in a turbulent fluid. *AIChE J.* **1957**, *3*, 381.

Friedlander, S. K. *Smoke, Dust and Haze*; Wiley-Interscience: New York, 1977.

Gardner, K. H.; Thomas, L. T. A unified kinetic model for particle aggregation. *J. Colloid Interface Sci.* **1996**, *180*, 162.

Garside, J. The concept of effectiveness factors in crystal growth. *Chem. Eng. Sci.* **1971**, *26*, 1425.

Garside, J. Industrial crystallization from solution. *Chem. Eng. Sci.* **1985**, *40*, 3.

Garside, J.; Tavare, N. S. Mixing, reaction and precipitation: Limits of micromixing in a MSMPR crystallizer. *Chem. Eng. Sci.* **1985**, *40*, 1485.

Giannetti, E. Nucleation mechanisms and particle size distributions of polymer colloids. *AIChE J.* **1993**, *39*, 1210.

Glendinning, A. B.; Russel, W. B. The electrostatic repulsion between charged spheres from exact solutions to the linearized Poisson−Boltzmann equation. *J. Colloid Interface Sci.* **1983**, *93*, 95.

Grant, M. L.; Saville, D. A. Electrostatic interactions between a nonuniformly charged sphere and a charged surface. *J. Colloid Interface Sci.* **1995**, *171*, 35.

Gruy, F.; Saint-Raymond, F. Turbulent coagulation efficiency. *J. Colloid Interface Sci.* **1997**, *185*, 281.

Hall, S. B.; Duffield, J. R.; Williams, D. R. A stochastic computer simulation of emulsion coalescence. *J. Colloid Interface Sci.* **1991**, *143*, 416.

Hogg, R.; Healy, T. W.; Fuerstenau, D. W. Mutual coagulation of colloidal dispersions. *Trans. Faraday Soc.* **1966**, *66*, 1638.

Honig, E. P.; Roebersen, G. J.; Wiersema, P. H. Effect of hydrodynamic interaction on the coagulation rate of hydrophobic colloids. *J. Colloid Interface Sci.* **1971**, *36*, 97.

Israelachvili, N. J. *Intermolecular and Surface Forces*; Academic Press: New York, 1985.

Koch, W.; Friedlander, S. K. The effect of particle coalescence on the surface area of a coagulating aerosol. *J. Colloid Interface Sci.* **1990**, *140*, 419.

Kostoglou, M.; Karabelas, A. J. Evaluation of zero order methods for simulating particle coagulation. *J. Colloid Interface Sci.* **1994**, *163*, 420.

Kostoglou, M.; Karabelas, A. J. Procedures for rapid calculation of the stability ratio of colloidal dispersions. *J. Colloid Interface Sci.* **1991**, *142*, 297.

Kostoglou, M.; Karabelas, A. J. Evaluation of numerical methods for simulating an evolving particle size distribution in growth processes. *Chem. Eng. Commun.* **1995**, *136*, 177.

Kostoglou, M.; Andritsos, N.; Karabelas, A. J. Flow of supersaturated solutions in pipes. Modeling bulk precipitation and scale formation. *Chem. Eng. Commun.* **1995**, *133*, 107.

Landgrebe, J. D.; Pratsinis, S. E. Gas-phase manufacture of particulates: Interplay of chemical reaction and aerosol coagulation in the free-molecular regime. *Ind. Eng. Chem. Res.* **1989**, *28*, 1474.

Lee, K. W. Conservation of particle size distribution parameters during Brownian coagulation. *J. Colloid Interface Sci.* **1985**, *108*, 199.

Levich, V. G. *Physicochemical Hydrodynamics*; Prentice Hall: New York, 1962.

Litster, J. D.; Smith, D. J.; Hounslow M. J. Adjustable discretized population balance for growth and aggregation. *AIChE J.* **1995**, *41*, 591.

Maetzing, H.; Baumann, W.; Paur, H. R. Bimodal aerosol coagulation with simultaneous condensation/evaporation. *J. Aerosol Sci.* **1996**, *27*, Suppl. 1, S363.

Marchal, P.; Marcant, B.; David, R.; Klein, J. P The modelling of agglomeration in industrial crystallization from solution. AIChE Annual Meeting, Los Angeles, Nov 1991.

McCabe, W. L.; Smith, J. C. *Unit Operations of Chemical Engineering*; McGraw-Hill: New York, 1967.

Megaridis, C. M.; Dobbins, R. A. A bimodal integral solution of the dynamic equation for an aerosol undergoing simultaneous particle inception and coagulation. *Aerosol Sci. Technol.* **1990**, *12*, 240.

Muhr, H.; David, R.; Villermaux, J.; Jezequel, P. H. Crystallization and precipitation engineering—V. Simulation of the precipitation of silver bromide octahedral crystals in a double-jet semibatch reactor. *Chem. Eng. Sci.* **1995**, *50*, 345.

Nadkarni, A. R.; Mahalingam, R. Aerosol behavior and concentration gradient fields in nonisothermal tube flow. *AIChE J.* **1985**, *31*, 603.

Nielsen, A. E. Diffusion controlled growth of a moving sphere. The kinetics of crystal growth in potassium perchlorate precipitation. *J. Phys. Chem.* **1960**, *65*, 46.

Nielsen, A. E. Electrolyte crystal growth kinetics. *J. Cryst. Growth* **1984**, *67*, 289.

Nitsche, J. M. On the asymptotic structure of far-field electrostatic interactions between charged molecules and charged surfaces. *Ind. Eng. Chem. Res.* **1996**, *35*, 3241.

Nylt, J.; Sohnel, O.; Matuchova, M.; Broul, M. *The Kinetics of Industrial Crystallization*; Elsevier: Amsterdam, The Netherlands, 1985.

Okuyama, K.; Huang, D.; Seinfeld, J. H.; Tani, N.; Kousaka, Y. Aerosol formation by rapid nucleation during the preparation of SiO_2 thin films from $SiCl_4$ and O_2 gases by CVD process. *Chem. Eng. Sci.* **1991**, *46*, 1545.

Papavergos, P. G.; Hedley, A. B. Particle deposition behaviour from turbulent flows. *Chem. Eng. Res. Dev.* **1984**, *62*, 275.

Papelis, C.; Hayes, K. F.; Leckie, J. O. *HYDRAQL*; Technical Report No. 306; Stanford University: Stanford, CA, 1988.

Park, H. M.; Rosner, D. E. Boundary layer coagulation effects on the size distribution of thermophoretically deposited particles. *Chem. Eng. Sci.* **1989**, *44*, 2225.

Phillips, R. J. Calculation of multisphere linearized Poisson—Boltzmann interactions near cylindrical fibers and planar surfaces. *J. Colloid Interface Sci.* **1995**, *175*, 386.

Pratsinis, S. E. Simultaneous nucleation, condensation, and coagulation in aerosol reactors. *J. Colloid Interface Sci.* **1988**, *124*, 416.

Press, W.; Flannery, B.; Teukolski, S.; Vetterling, W. *Numerical Recipes*; Cambridge University Press: New York, 1986.

Prieve, D. C.; Lin, M. M. J. The effect of the distribution of surface properties on colloid stability. *J. Colloid Interface Sci.* **1982**, *86*, 17.

Randolph, A. D.; Larson, M. A. *Theory of Particulate Processes*; Academic Press: New York, 1971.

Reddy, S. R.; Melik, D. H.; Fogler, H. S. Emulsion stability—Theoretical studies on simultaneous flocculation and creaming. *J. Colloid Interface Sci.* **1981**, *82*, 116.

Rosner, D. E.; Tassopoulos, M. Deposition rates from polydispersed particle populations of arbitrary spread. *AIChE J.* **1989**, *35*, 1497.

Ruckenstein, E.; Prieve, D. C. Rate of deposition of Brownian particles under the action of London and double layer forces. *J. Chem. Soc., Faraday Trans. 2*, **1973**, *69*, 1522.

Russel, W. B.; Saville, D. A.; Schowalter, W. R. *Colloidal Dispersions*; Cambridge University Press: Cambridge, U. K., 1989.

Sader, J. E.; Carnie, S. L.; Chan, D. Y. C. Accurate analytic formulas for the double layer interaction between spheres. *J. Colloid Interface Sci.* **1995**, *171*, 46.

Saffman, P. G.; Turner, J. J. On the collision of drops in turbulent clouds. *J. Fluid Mech.* **1956**, *1*, 16.

Seckler, M. M.; Bruinsma, O. S. L.; Van Rosmalen, G. M. Influence of Hydrodynamics on precipitation: A computational study. *Chem. Eng. Commun.* **1995**, *135*, 113.

Smith, J. M. *Chemical Engineering Kinetics*; McGraw-Hill: New York, 1981.

Sohnel, O.; Garside, G. *Precipitation. Basic Principles and Industrial Applications*; Butterworth-Heinemann: Oxford, U.K., 1992.

Spielman, L. A. Viscous interactions in Brownian coagulation. *J. Colloid Interface Sci.* **1970**, *33*, 562.

Spielman, L. A.; Friedlander, S. K. Role of the electrical double layer in particle deposition by convective diffusion. *J. Colloid Interface Sci.* **1974**, *46*, 22.

Tandon, P.; Rosner, D. E. Co-deposition on Hot CVD surfaces: Particles dynamics and deposit roughness interactions. *AIChE J.* **1996**, *42*, 1673.

Tang, Z.; Mier-y-Teran, L.; Davis, H. T.; Scriven, L. E.; White, H. S. Non-local free energy density-functional theory applied to the electrical double layer. *Mol. Phys.* **1990**, *71*, 369.

Tavare, N. S. Mixing in continuous crystallizers. *AIChE J.* **1986**, *32*, 705.

Tsai, K.; Fox, R. O. PDF modeling of turbulent mixing effects on initiator efficiency in a tubular LDPE reactor. *AIChE J.* **1996**, *42*, 2926.

Tsang, T. H.; Rao, A. Comparison of different numerical schemes for condensational growth of aerosols. *Aerosol Sci. Technol.* **1988**, *9*, 271.

Tsouris, C.; Scott, T. C. Flocculation of paramagnetic particles in a magnetic field. *J. Colloid Interface Sci.* **1995**, *171*, 319.

Vasak, F.; Bowen, B. D.; Chen, C. Y.; Kastanek, F.; Epstein, N. Fine particle deposition in laminar and turbulent flows. *Can. J. Chem. Eng.* **1995**, *73*, 785.

Verwey, E. J. W.; Overbeek, J. T. G. *Theory of the Stability of Lyophobic Colloids*; Elsevier: Amsterdam, The Netherlands, 1948.

Villadsen, J.; Michelsen, M. L. *Solution of Differential Equation Models by Polynomial Approximation*; Prentice-Hall: New York, 1978.

Wachi, S.; Jones, A. G. Mass transfer with chemical reaction and precipitation. *Chem. Eng. Sci.* **1991**, *46*, 1027.

Williams, M. M. R. On the modified Gamma distribution for representing the size spectra of coagulating aerosol particles. *J. Colloid Interface Sci.* **1985**, *103*, 516.

Williams, M. M. R.; Loyalka, S. K. *Aerosol Science*; Pergamon Press: New York, 1991.

Xiong, Y.; Pratsinis, S. E. Gas-phase production of particles in reactive turbulent flow. *J. Aerosol Sci.* **1991**, *22*, 637.

Xiong, Y.; Pratsinis, S. E.; Mastrangelo, S. V. R. The effect of ionic additives on aerosol coagulation. *J. Colloid Interface Sci.* **1992**, *153*, 106.

Yuu, S. Collision rate of small particles in a homogeneous and isotropic turbulence. *AIChE J.* **1984**, *30*, 802.

Zukoski, C. F.; Rosenbaum, D. F.; Zamora, P. C. Aggregation in precipitation reactions: Stability of primary particles. *Trans. Inst. Chem. Eng.* **1996**, *74A*, 723.

Received for review August 13, 1997
Revised manuscript received January 9, 1998
Accepted January 13, 1998

IE970559G